Advanced Composite Materials
Publication details, including instructions for authors and subscription information:
http://www.tandfonline.com/loi/tacm20

Noise and vibration reduction technology in aircraft cabins

Kosaku Takahashi , Hirotaka Monzen , Toshihiro Yamaoka , Koji Kusumoto , Kazuhiro Bansaku , Jyunichi Kimoto , Akira Isoe , Yasuo Hirose , Tomio Sanda & Yuji Matsuzaki

Version of record first published: 02 Apr 2012.

To cite this article: Kosaku Takahashi , Hirotaka Monzen , Toshihiro Yamaoka , Koji Kusumoto , Kazuhiro Bansaku , Jyunichi Kimoto , Akira Isoe , Yasuo Hirose , Tomio Sanda & Yuji Matsuzaki (2004): Noise and vibration reduction technology in aircraft cabins, Advanced Composite Materials, 13:1, 67-80

To link to this article: http://dx.doi.org/10.1163/1568551041408787

Adv. Composite Mater., Vol. 13, No. 1, pp. 67–80 (2004)

Also available online - www.vsppub.com

Noise and vibration reduction technology in aircraft cabins

KOSAKU TAKAHASHI [1,*], HIROTAKA MONZEN [1], TOSHIHIRO YAMAOKA [1], KOJI KUSUMOTO [1], KAZUHIRO BANSAKU [1], JYUNICHI KIMOTO [1], AKIRA ISOE [1], YASUO HIROSE [1], TOMIO SANDA [1] and YUJI MATSUZAKI [2]

[1] *Aerospace Company, Kawasaki Heavy Industries Ltd., 1 Kawasaki-Cho, Kakamigahara City, Gifu-Pref., 504-8710, Japan*

[2] *Graduate School of Engineering, The University of Nagoya, 1 Furho-cho, Chikusa-ku, Nagoya, 464-8603, Japan*

Received 18 July 2003; accepted 22 March 2004

Abstract—This study investigates how to reduce noise and vibration in aircraft cabins with $Pb(TiZr)O_3$ (PZT), using a semi-monocoque structure 1.5 m in diameter and 3.0 m long with a 2.3 mm skin, which simulates an aircraft body. We utilized 480 pieces of PZT bonded on the inner surface of the structure as sensors and actuators. We applied random noise in the low frequency range from 0 to 500 Hz to the test model. By controlling the PZTs, we tried to reduce the vibration level of the structure and the internal air due to the external load.

Two control methods, gain control and feed-forward control, were tried. We measured internal sound pressure at 150 points and compared the overall values of sound pressure with gain control to those without control and evaluated the reduction capabilities. The tests demonstrated a maximum 4.0 dB O.A. reduction with gain control and a maximum 3.5 dB O.A. reduction with feed-forward control.

Keywords: PZT; vibration control; acoustic control; C/Ep composite.

1. INTRODUCTION

Sound absorption material for cabin noise reduction is conventionally used in aircraft. It requires much space and is effective in the high-frequency range, but less effective in the low- frequency range due to longer wavelengths that exceed the thickness of the absorbing materials. While the current passive noise control is still good in high-frequency ranges, active noise control is desirable in the low-frequency

*To whom correspondence should be addressed at Aerospace Engineering Department, Engineering Division, Aerospace Company, Kawasaki Heavy Industries Ltd., 1 Kawasaki-Cho, Kakamigahara City, Gifu-Pref., 504-8710, Japan. E-mail: takahashi_k@khi.co.jp

ranges. This idea inspired many studies using PZT on an elemental level like a plate. Two years ago, we studied the radiated sound power reduction capability of PZT in low frequency ranges with 600 mm × 600 mm × 2.0 mm CFRP board [1]. Recently, there have been many studies on internal noise reduction, utilizing a model that simulates aircraft body structures [2].

In this study, we built a 1/3-scale model of an aircraft fuselage and implemented noise and vibration reduction tests in a wide range of low frequencies. This paper will outline the test model, tests and the results.

2. TEST MODEL

2.1. Test model configuration and details

We built a test model that simulated a small aircraft fuselage structure, scaled to one-third. Figure 1 illustrates the test model.

The test model is a cylindrical structure, 1.5 m in diameter and 3.0 m long, with a 2.3 mm skin of composite (CFRP), which has aluminum alloy bulkheads on both sides. Also, it has four stringers evenly spaced and five aluminum alloy frames with 750 mm spacing. The body is made of 16 curved panels of carbon/epoxy laminate fabric; the laminates are 12 plies [(0, 90)/(±45)/(0, 90)/(±45)/(0, 90)/(±45)]s. The panels are fastened to the stringers and frames.

We assembled a simple calculation model of a small aircraft and calculated the vibration properties of the structure and internal air. From the vibration properties of the calculation model, we were able to derive the number and the size of panels, frames and stringers in the test model.

2.2. Vibration characteristics of the test model and internal air

In order to confirm vibration characteristics of the test model structure and the internal air in frequencies from 0 to 500 Hz, we performed vibration analysis by

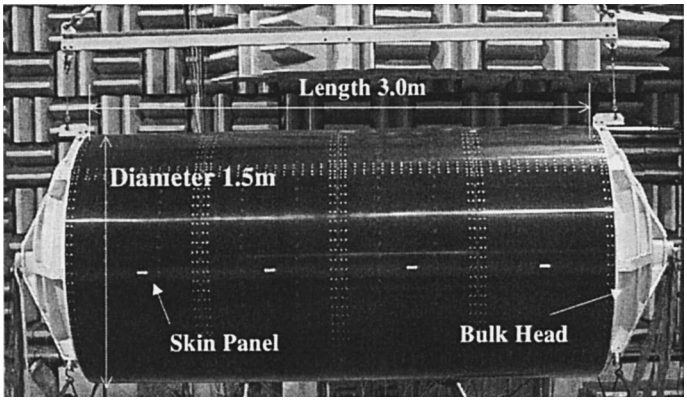

Figure 1. Test model photograph.

NASTRAN and a vibration test. The frequency range from 0 to 500 Hz was the control target. In the vibration analysis, the structure and air were analyzed independently. The analysis model was improved by using the results of that test. We found 301 vibration modes and 105 air vibration modes within the 0 to 500 Hz range. Figure 2 depicts an FEM model of structure and air used in the calculations.

Table 1.
Vibration characteristics of test model

Mode No.	Structure			Internal air		
	Nastran (Hz)	Test results (Hz)	Error	Nastran (Hz)	Test results (Hz)	Error
1	106.4	90.0	15.4%	53	54	−1.5%
2	110.1	90.1	18.2%	106	106	−0.4%
3	115.4	98.0	15.1%	137	139	−1.5%
4	116.8	96.8	17.2%	150	151	−0.7%
5	131.9	133.0	−0.8%	157	158	−0.5%
6	132.8	137.5	−3.5%	178	179	−0.3%
7	133.0	137.6	−3.5%	206	209	−1.5%
8	141.8	144.6	−1.9%	216	216	−0.1%
9	142.0	141.0	0.7%	225	231	−2.6%
10	143.9	157.5	−9.4%	235	226	3.8%
11	175.4	169.5	3.4%	246	246	0.3%
12	184.1	186.8	−1.4%	260	262	−1.0%

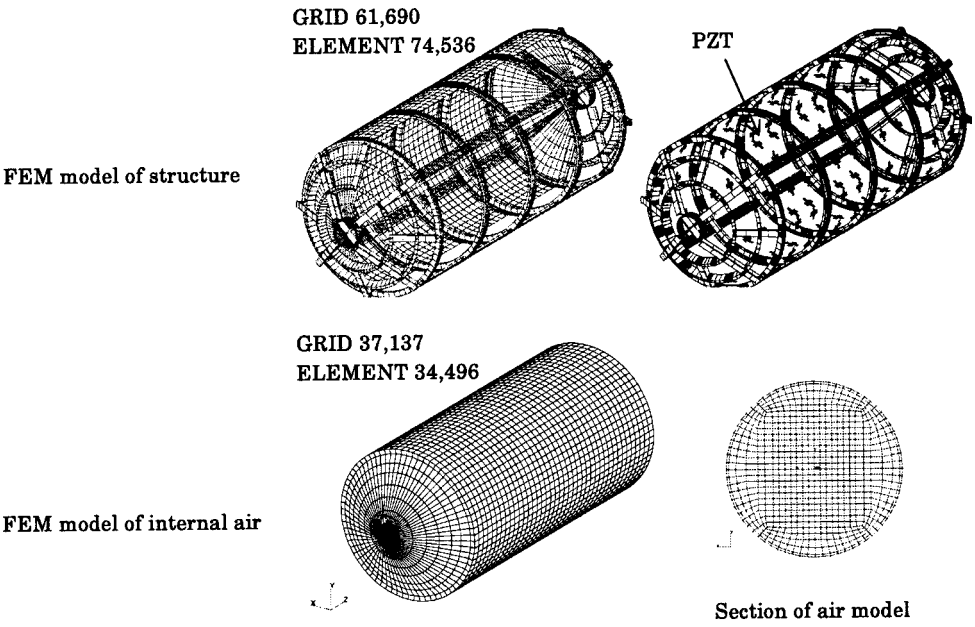

Figure 2. Analysis model of test model (NASTRAN FEM MODEL).

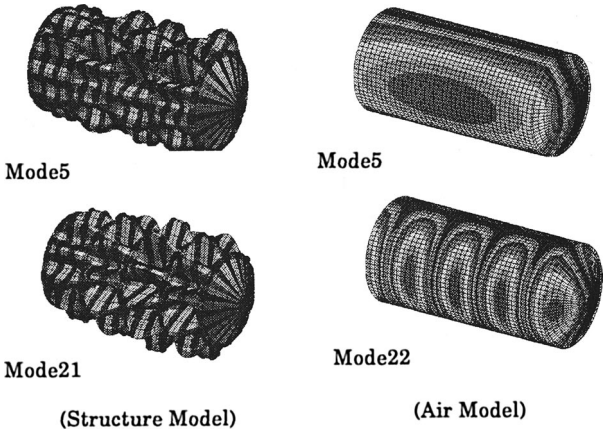

Figure 3. Vibration mode of test model.

Table 1 gives the characteristics of vibration from the 1st to 12th vibration modes (also see Fig. 3).

2.3. PZT layout

When you try to suppress the structural vibration of panels or make the panels vibrate for use as speakers in order to control the internal sound pressure, it is a good idea to locate the PZT at the place where you can control the structural vibration mode that most affects the internal sound pressure. This idea determined the PZT layout.

The vibration mode of induced internal air induced was calculated by exciting the test model on one side with an external sound source while we checked the relation of each structure vibration mode with the air vibration mode. Figure 4 presents the calculation results. In Fig. 4, we selected the structural vibration modes that most affect internal sound pressure and studied the layout of PZT considering the shapes of the structure vibration modes. Figure 5 illustrates the final layout of PZT after our study. The PZT configuration was 40 mm $\times$ 30 mm $\times$ 0.5 mm. The PZT was manufactured by Fuji Ceramics Co. Sets with 5 PZTs were bonded to the inside surface of the CFRP panels using epoxy adhesive. The center PZT was used as a sensor and the rest were used as actuators. Each panel had six sets of PZTs, which amounted to 480 pieces of PZT in the test model, as shown in Fig. 6.

3. EQUATION OF MOTION FOR THE TEST MODEL

To determine the control method and the control parameter, we simulated the effect of control using a numerical model. The equations used in the simulation are described below.

The equation of motion for the test model with PZT and internal air is shown in equation (1) in modal coordinates. The left side corresponds to the coupling of the

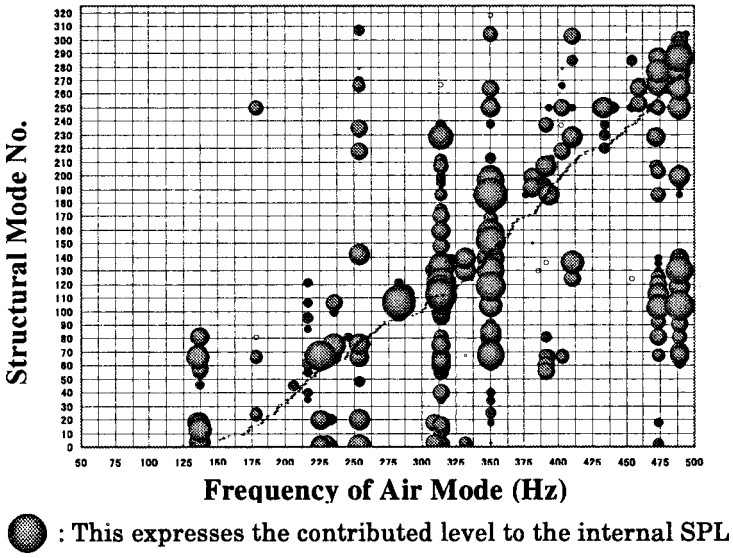

Figure 4. Relation between internal sound pressure and vibration mode.

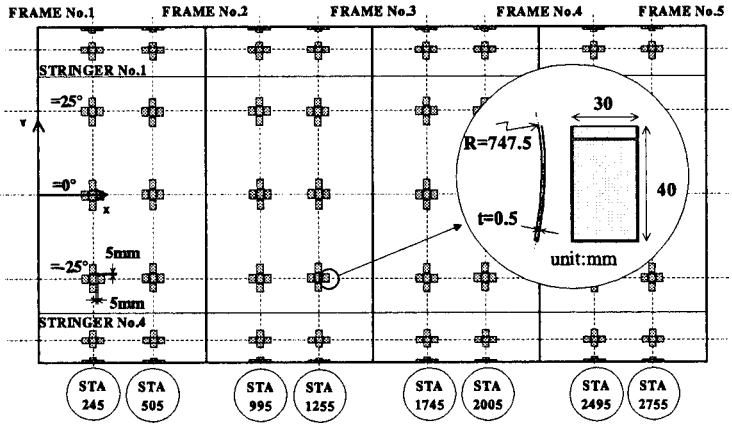

Figure 5. PZT layout.

structure with air. From the right, the first term presents the control force of PZT and the second term is the external force used to excite the modes.

$$\begin{bmatrix} M_s & 0 \\ A_{sf} & M_f \end{bmatrix} \begin{Bmatrix} \ddot{u}_s \\ \ddot{u}_f \end{Bmatrix} + \begin{bmatrix} B_s & 0 \\ 0 & B_f \end{bmatrix} \begin{Bmatrix} \dot{u}_s \\ \dot{u}_f \end{Bmatrix} + \begin{bmatrix} K_s & -A_{sf}^T \\ 0 & K_f \end{bmatrix} \begin{Bmatrix} u_s \\ u_f \end{Bmatrix} = \begin{bmatrix} f_{pzt} \\ 0 \end{bmatrix} \{u\} + \begin{bmatrix} f_s \\ 0 \end{bmatrix} \{w\}. \quad (1)$$

Here u_s, u_f are the modal displacement vectors, and M_s, B_s, and K_s are the generalized mass matrix, damping matrix and stiffness matrix of the structure. M_f,

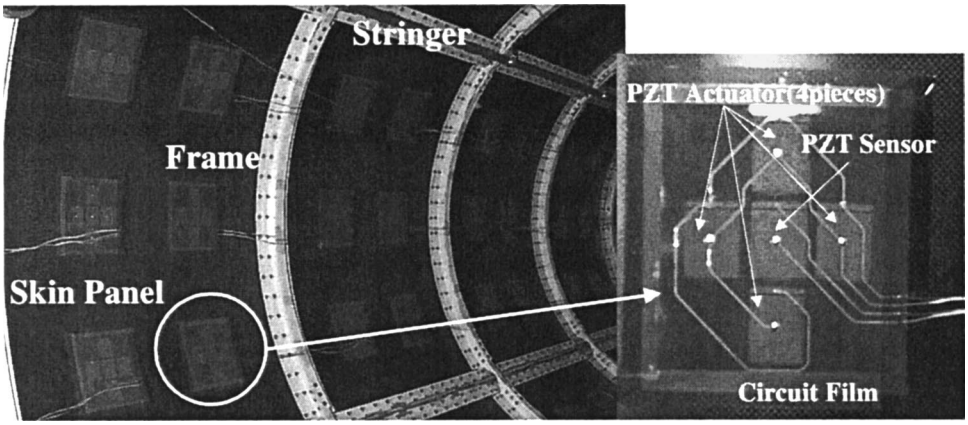

Figure 6. Photo of PZT and wiring layout.

B_f, and K_f are the generalized mass matrix, damping matrix and stiffness matrix of air. A_{sf} is the influence matrix of the structure and air, u is the control voltage vector, f_{pzt} is the generalized external force matrix applied by PZT, w is the input signal to an exciter, and f_s is the generalized external force vector applied to the structure by an exciter.

In-plane deformations of PZT were used as actuators in this study. In-plane strains ε_1, ε_2 due to input of voltage V are given by equation (2):

$$\varepsilon_1 = \varepsilon_2 = d_{31} V/t, \tag{2}$$

where t is the PZT thickness and d_{31} is the piezoelectric charge constant. Assuming the applied voltage V as temperature and the d_{31}/t as a thermal expansion coefficient in the above equation (2), the active force applied by PZT actuators on the CFRP panel can be derived in the same manner as the thermal stress analysis of the finite element method. When we use NASTRAN thermal stress analysis, equation (2) yields

$$f_{pzt} = [\phi_s][K_e]\{V\}, \tag{3}$$

where matrix $[K_e]$ is the force applied to each structure node due to unit voltage applied to PZT and $[\phi_s]$ is the matrix composed of structural eigenvectors. Also, for plane stress, the relation between in-plane strain ε_1, ε_2 due to structural deformation and voltage V_{pzt} from PZT is given by

$$\varepsilon_1 + \varepsilon_2 = -\frac{1-\nu}{g_{31} E t} V_{pzt}, \tag{4}$$

where g_{31} is the piezoelectric voltage constant and E and ν are Young's modulus and Poisson's ratio for PZT. Equation (4) converts the output voltage of PZT to the strain $\varepsilon_1 + \varepsilon_2$ on PZT due to structural deformation. As the strain value of PZT due to each vibration mode of the structure can be obtained from the real eigenvalue analysis, we are able to relate $\varepsilon_1 + \varepsilon_2$ of equation (4) to modal deformation u_s of the

structure, as in

$$\varepsilon_1 + \varepsilon_2 = [K_\varepsilon]\{u_s\}, \tag{5}$$

where matrix $[K_\varepsilon]$ is derived from the relation of the strain value of PZT and structural vibration modes.

We can make an analytical model of the actuators and sensor using equations (3) and (4). From equation (1), the state equation, which takes the combined effect of structure, internal air and PZT actuator into account, is given as follows.

$$\begin{aligned} \dot{x} &= Ax + B_{pzt}u + B_s w, \\ x &= \{\dot{u}_s \dot{u}_f u_s u_f\}^T. \end{aligned} \tag{6}$$

Assuming the status value as x, strain y_{pzt} measured through the PZT and internal sound pressure y_p of the test model are expressed as in equations (7) and (8).

$$y_{pzt} = C_{pztstrain}x, \tag{7}$$

$$y_p = C_p x. \tag{8}$$

Matrix C_p in (8) is made from the peculiar vibration mode matrix of air. We conducted control simulations by MATLAB using (7) and (8) to find how much we could reduce noise and vibration.

4. NOISE AND VIBRATION CONTROL TEST ARRANGEMENT

4.1. Test arrangement

A noise and vibration control test was conducted, using the test model slung in an anechoic room. Figure 7 illustrates the test set-up. The test system was composed of speakers to vibrate the test model, measurement instruments for vibrations of the test model, and an internal noise and control system (DSP) for sending signals to actuators after calculating the control voltage from sensor signals.

To evaluate the effect of control, we measured the acceleration of the panel and internal sound pressure. Eighteen accelerometers were attached to the surface of the panel. We moved 15 microphones fixed on microphone support tools with a 150 mm spacing and measured internal sound pressure at 150 points. The measured data of the acceleration and internal sound pressure are Power Spectrum Density (PSD) and the overall value in the frequency range of 20 to 500 Hz.

4.2. Test condition

The test model was excited by two external speakers that were located 1 m from the model and driven to generate noise through input signals. We used a random signal (white noise) of 0 to 512 Hz as input and loaded random noise into the model. Figure 10 depicts the measured values of sound pressure on the surface of the test

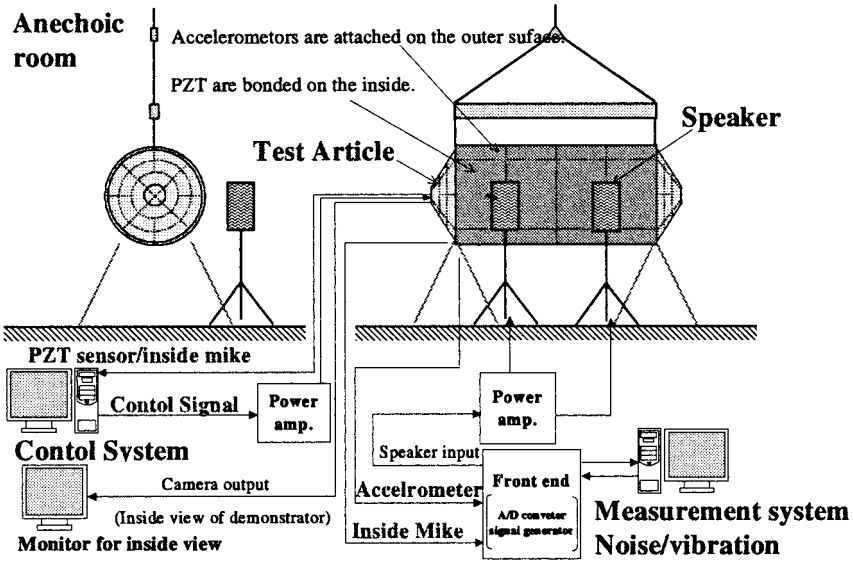

Figure 7. Test arrangement.

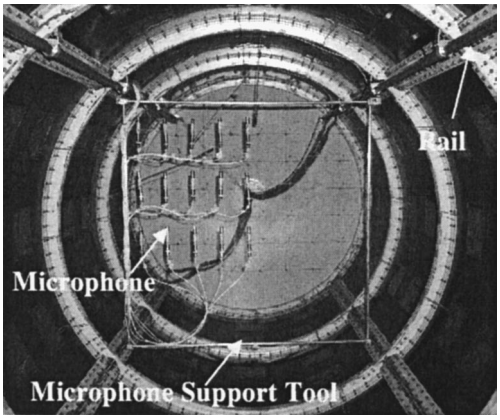

Figure 8. Measurement arrangement of internal sound pressure.

model. A maximum sound pressure of 107 dB O.A. was detected at the center on the side of the model.

5. NOISE AND VIBRATION CONTROL TESTS

Two control methods were used to control vibration and noise. They are gain control and feed-forward control. The test methods and test results of each control method are shown below.

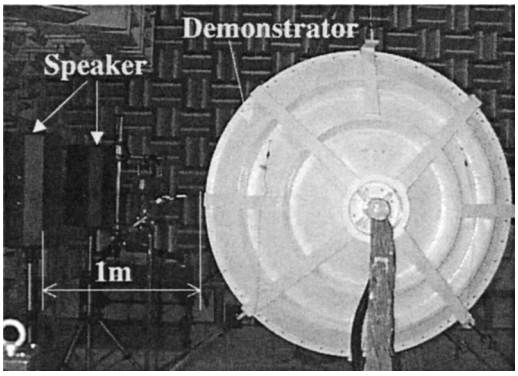

Figure 9. External forcing vibration.

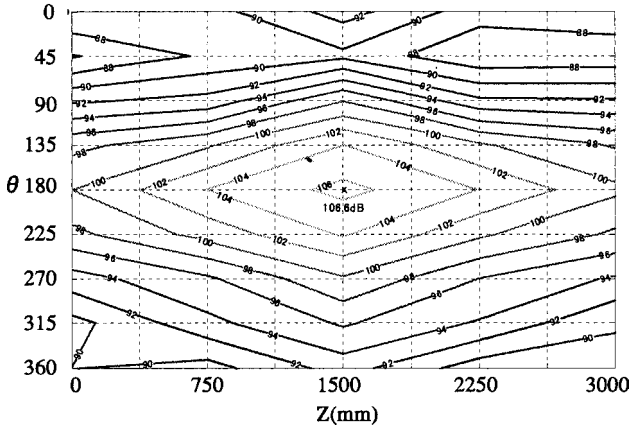

Figure 10. Sound pressure distribution on model surface.

5.1. Gain control test

We tried to reduce the vibration of the panel through a gain control method since the reduction of panel vibration was expected to suppress the internal sound pressure. Figure 11 shows the control system gain control diagram.

During gain control, the PZT output voltage for the sensor multiplied by the strain transform coefficient K_{pzt} is transformed to strain and after gain multiplication (K_{gain}), weight function $G_w(s)$ for adjusting phase and magnitude will be multiplied in order to increase the control effect in the frequency range for control. It will then be fed back to the PZT actuators as control voltage u. The relation between PZT output voltage V_{pzt} for the sensor and control voltage u is shown in equation (9).

$$u = G_w(s) K_{gain} K_{pzt} V_{pzt}. \tag{9}$$

Control simulation studies determined the weight function $G_w(s)$ and gain constant K_{gain}.

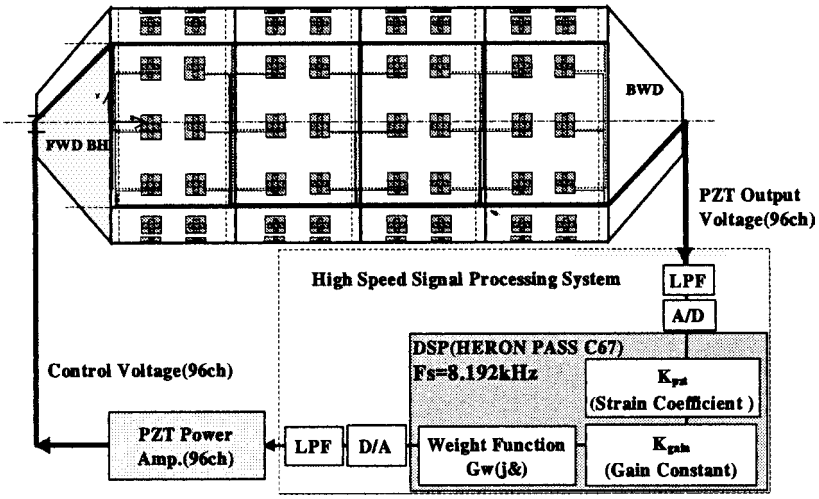

Figure 11. Control system diagram (with gain control).

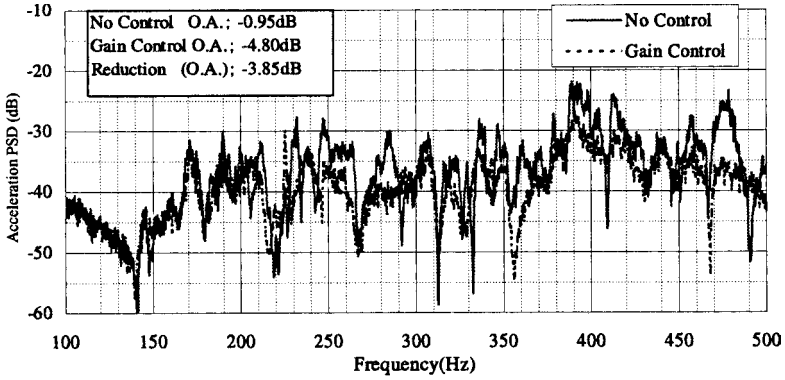

Figure 12. PSD of acceleration on the panel (with gain control).

The results of the gain control tests in which we used 96 PZTs as sensors and 96 sets of PZT (384 pieces) as actuators will be detailed below. In control, we used strain transform coefficients $K_{pzt} = 3.03 \times 10^6$, gain constants $K_{gain} = -3.5 \times 10^7$, weight function $G_w(s)$ of the first Butterworth filter and a sampling frequency of 8.192 Hz.

PSD distributions of the accelerations with gain control and without gain control are compared in Fig. 12 in order to the evaluate vibration control capability. We can see much control capability at the natural frequency of the vibration mode of the panel from 200 to 500 Hz and get an acceleration reduction of 5 to 10 dB at peak and 3.9 dB for 20 to 500 Hz O.A.

In order to evaluate the control capability for internal noise levels, internal sound pressure was measured at 150 points inside the test model, both with and without control. We calculated the overall sound pressure from 200 to 500 Hz for each case

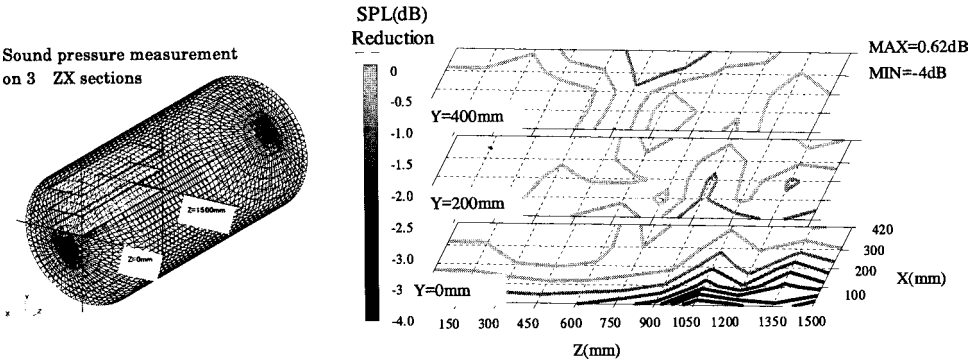

Figure 13. Internal sound pressure reduction distribution (with gain control).

and show the difference in Fig. 13, where one can see a maximum reduction of 4 dB in the sound pressure level. Since the reduction rate estimated through our control simulation was 3.6 dB, the 4 dB reduction attained in the present demonstration is reasonable.

5.2. Feed-forward control test

Feed-forward control is a method to force the test model panels to vibrate and induce sound inside the test model (instead of using speaker control), when we try to reduce the internal sound pressure.

Figure 14 illustrates our control system diagram for feed-forward control. The error sensors are three microphones placed inside the test model. The reference input is taken from a microphone placed at the front of the speaker.

After changing the coefficient of an adjusting filter by the Filtered-X LMS (least mean square) Algorithm [3, 4] from an error sensor, reference input, and control voltage, the system will determine the control voltage to suppress the air mode monitored by an error sensor.

We selected three greater air vibration modes during forced vibration and determined the layout of error sensors so that we were able to measure each mode easily. The PZT actuators were grouped so that they could control the selected air mode. The mode shape of sound pressure helped to arrange three groups of PZT actuators. Figure 15 depicts the air vibration modes to be controlled, and Fig. 16 illustrates how groups of PZT actuators were arranged. We tried to reduce internal sound pressure by doing three independent controls of the Single Input Single Output (SISO) system simultaneously.

When the sound pressure radiated from external speakers and body panels forced by PZT actuators are d_k, y_k, at the sensor point, the sound pressure that sensor will measure is given by

$$\begin{aligned} e_k &= d_k + y_k \\ &= d_k + \mathbf{G}u_k, \end{aligned} \tag{10}$$

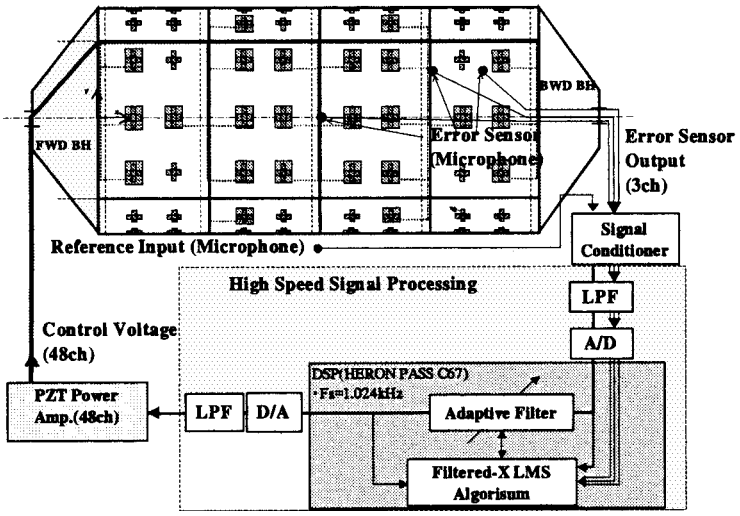

Figure 14. Feed-forward control system diagram.

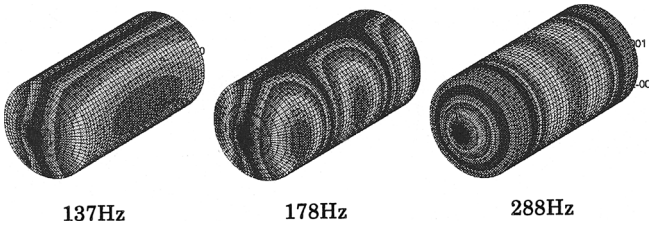

Figure 15. Air vibration mode to be controlled.

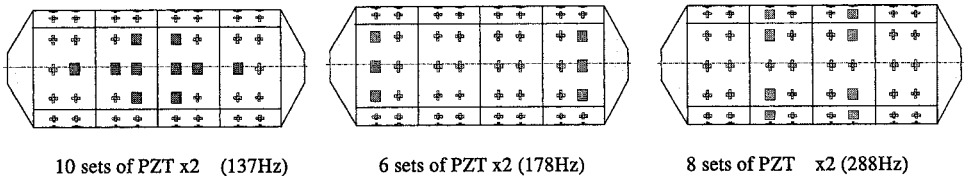

Figure 16. Groups of PZT actuators (Feed-forward control).

where u_k is the control voltage and **G** is the transfer-function of sound pressure from the input voltage of PZT actuators to the error sensor point. The transfer-function was measured by test. Control voltage u_k was given in the form of a IIR filter by equation (11). We controlled the system, while changing the filter coefficient vectors **a**, **b** of feedback and feed-forward through a Filtered-X LMS algorithm to minimize $E[e_k^2]$.

$$u_k = \mathbf{a} * x_k + \mathbf{b} * u_{k-1}, \tag{11}$$

x_k reference signal.

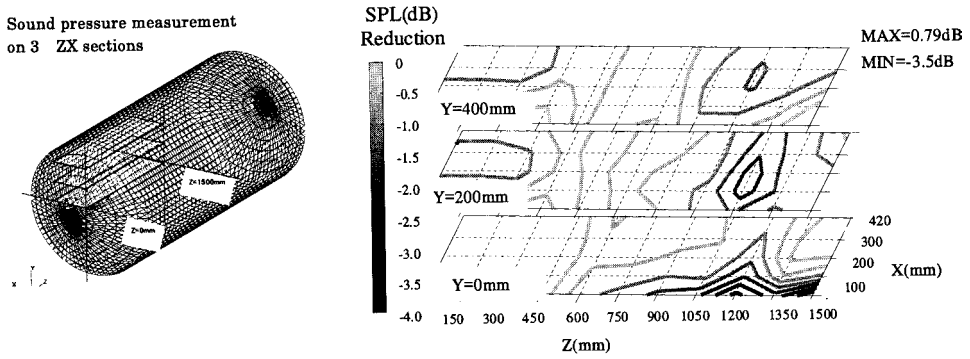

Figure 17. Internal sound pressure reduction distribution (with Feed-forward control).

The test results of feed-forward control will follow. The test was performed with 14th order and 15th order filter length of the filter coefficient vectors **a**, **b**. The sampling frequency was 1024 kHz.

In order to evaluate control capability for internal noise levels, we measured the internal sound pressure with and without control at 150 points inside the test model. We calculated the overall sound pressure from 20 to 500 Hz for each case and are present their difference in Fig. 17, where there is a maximum reduction of 3.5 dB in sound pressure level. The estimated reduction in our control simulation was 6 dB, but the test yielded lower performance. In the test, three air vibration modes were reduced by 10 dB (peak) as shown in the estimation, but we found that the other air vibration modes could not be controlled and increased sound pressure.

6. CONCLUSION

We built a 1/3-scale semi-monocoque test model, 1.5 m in diameter and 3.0 m long with 2.3 mm skin to simulate an aircraft fuselage and conducted internal noise and vibration control tests using 480 PZTs.

We applied two control methods, gain control and feed-forward control; the test results confirmed a reduction of 4.0 dB O.A. for gain control and 3.5 dB O.A. for feed-forward control.

In gain control, the calculation time delay due to DSP prevented the gain from increasing. An analog circuit without the time delay would increase reduction capability. Also, in feed-forward control, increasing the number of air vibration modes for control would help increase the reduction capability. We have a few items to be improved, such as system miniaturization and actuator capability. However, we are sure that we can establish the basic technology for cabin-noise reduction.

Acknowledgements

This study has been conducted as a part of the 'R&D for Smart Materials and Structures System' project within the Academic Institutions Centered Program

supported by the New Energy and Industrial Technology Development Organization (NEDO) of Japan.

REFERENCES

1. K. Takahashi, K. Bansaku, T. Sanda and Y. Matsuzaki, Sound and vibration control tests of composite panel using piezoelectric sensors and actuators, in: *SPIE*, Vol. 4327, pp. 680–687 (2001).
2. C. A. Savran, M. J. Atalla and S. R. Hall, Broadband active structural-acoustic control of fuselage test-bed using collocated piezoelectric sensors and actuators, in: *SPIE*, Vol. 3984, pp. 135–147 (2000).
3. A. Nagamatsu, *Mode Analysis and Control of Sound and Vibration*. Korona's Publishing Co. (1996).
4. W. Xu, B. Leigh, A. Grewall, L. Pavel and D. G. Zimcik, Application of feedforward and feedback structural control for aircraft cabin noise reduction, in: *AIAA 98-1979*, pp. 2265–2275 (1998).